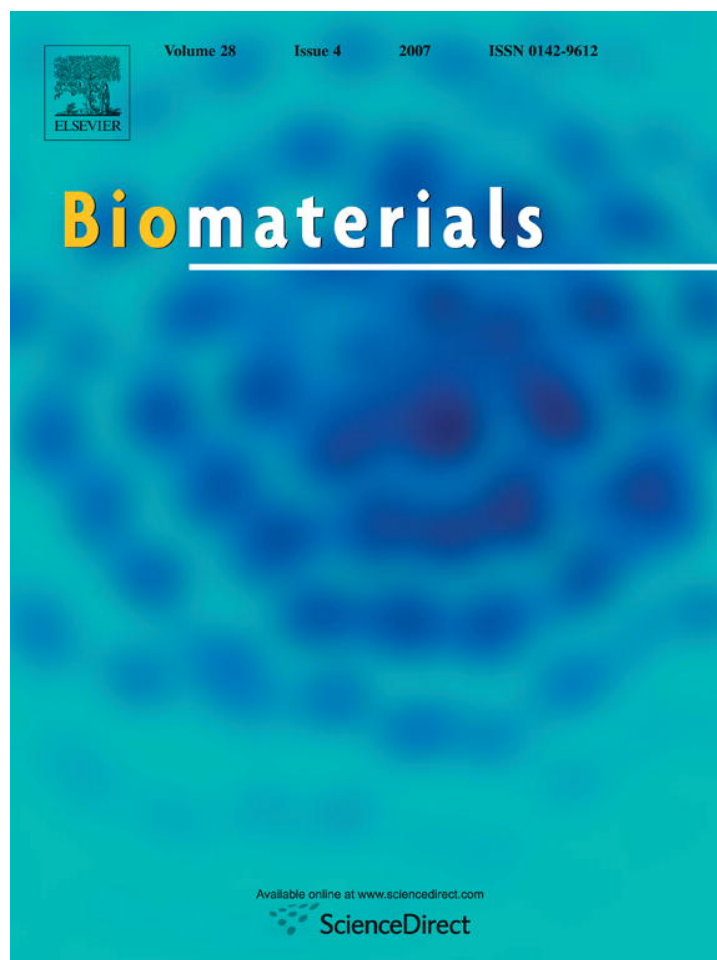


Provided for non-commercial research and educational use only.
Not for reproduction or distribution or commercial use.



This article was originally published in a journal published by Elsevier, and the attached copy is provided by Elsevier for the author's benefit and for the benefit of the author's institution, for non-commercial research and educational use including without limitation use in instruction at your institution, sending it to specific colleagues that you know, and providing a copy to your institution's administrator.

All other uses, reproduction and distribution, including without limitation commercial reprints, selling or licensing copies or access, or posting on open internet sites, your personal or institution's website or repository, are prohibited. For exceptions, permission may be sought for such use through Elsevier's permissions site at:

<http://www.elsevier.com/locate/permissionusematerial>

In vitro fatigue–crack growth and fracture toughness behavior of thin-walled superelastic Nitinol tube for endovascular stents: A basis for defining the effect of crack-like defects

Scott W. Robertson, Robert O. Ritchie*

Department of Materials Science and Engineering, University of California, Berkeley, CA 94720, USA

Received 28 July 2006; accepted 26 September 2006

Available online 10 October 2006

Abstract

Endovascular stents made of the superelastic nickel-titanium alloy Nitinol are subjected in service to tens of millions of loading cycles and even “single-event” overloads, both of which can potentially result in fracture and/or complete failure of the device. A fracture-mechanics-based methodology can provide a means to quantify relevant material parameters critical to the design against such failures. However, there is a dearth of relevant experimental data in the literature on such fracture-mechanics-based approaches to fatigue in Nitinol; furthermore, that which does exist invariably pertains to product forms that are not appropriate for stent manufacture, e.g., bulk Nitinol bar and strip. Consequently, the current work is focused on characterizing in vitro both subcritical and critical crack growth (fatigue–crack growth and *R*-curve fracture toughness) behavior in thin-walled (~400 μm thick) Nitinol tubing similar to that used for medical device manufacture (following shape-setting procedures to flatten the material), with a resultant austenite finish temperature of $A_f \sim 25\text{--}30^\circ\text{C}$, identical to self-expanding Nitinol stents. Fatigue–crack growth behavior, measured in Hanks’ Balanced Saline Solution over a wide spectrum of growth rates (down to 10^{-10} m/cycle) and at a range of positive load ratios ($R = 0.1\text{--}0.7$), revealed significantly higher fatigue thresholds than had been previously reported for bulk Nitinol material. In addition, we examine the critical effect of test frequency, as most fatigue experiments on Nitinol have been performed at 30 Hz or above, despite the fact that this is far in excess of the frequency of physiological loading. Finally, the fracture toughness properties are characterized in thin-section Nitinol and show marked crack-resistance (*R*-curve) behavior with a dependence on crack-growth angle (with respect to the tube drawing axis); additionally, measured toughnesses are found to be lower than has been previously reported for bulk Nitinol.

© 2006 Elsevier Ltd. All rights reserved.

Keywords: Fatigue; Fracture toughness; Fracture mechanism; Nitinol; Nickel-titanium alloy; Stent

1. Introduction

Nitinol, a nearly equiatomic alloy of Ni and Ti, has many useful characteristics (e.g., superelasticity, corrosion resistance, etc.) that make it particularly favorable for the fabrication of endovascular stents. Such stents are generally manufactured by precision laser machining of deep-drawn thin-walled tubes (typically several hundred micrometers thick), followed by multiple heat treatment steps to “train” the device to its desired configuration. Stresses from implantation and in vivo operation subject stents to a

variety of overload and cyclic stresses, for example from flexions of the joints and the systolic/diastolic sinus rhythms of the blood vessels, which can lead to “single-event” overload fracture and/or fatigue damage; damage can potentially result in degraded performance or, in the worse-case scenario, complete failure of the device. Despite the recognized importance of this issue, the basic fatigue–crack growth and fracture toughness of Nitinol tubing is neither well documented nor understood. The majority of prior research on Nitinol fatigue has focused on determining the stress/strain-life (*S–N*) properties of wire and stent-like samples [1–11]. Although vital in determining safe-operating mean and alternating stresses and strains in Nitinol devices, such *S–N* properties do not reveal the

*Corresponding author. Tel.: +1 510 486 5798; fax: +1 510 486 4881
E-mail address: roritchie@lbl.gov (R.O. Ritchie).

individual contributions from the crack nucleation and crack growth, which are critical in estimating conservative device lifetimes and determining critical flaw size detection limits. In particular, a fracture-mechanics based (so-called damage-tolerant) characterization of the fatigue and fracture behavior, which compliments existing total-life data and life-prediction analyses, is crucial from the perspective of defining the effect (in terms of potential fracture or reduced lives) of pre-existing crack-like defects in the device; *S/N* analyses alone can give little indication of such defect-induced fracture risks (see Ref. [12] for such an analysis). However, fatigue–crack propagation data for Nitinol are extremely limited; in fact, to our knowledge, there have only been four previous studies which isolate crack-growth phenomena in this material, and the majority of this work involves Nitinol product forms that are inappropriate for the manufacture of endovascular stents, namely 40 mm diameter bar [13,14] and 200 μm thin strip [15]). Moreover, virtually all experimental studies on the fatigue of Nitinol have been conducted at frequencies far in excess of physiological loading, and to date the effect of frequency on fatigue–crack growth remains undefined. Only one study [16], by the current authors, reports fatigue–crack growth in Nitinol tube material suitable for endovascular stents at both low and high frequencies (5–50 Hz); however, these experiments still did not address frequencies as low as those seen in vivo (~ 1 Hz) and further were only conducted at a few ΔK values. The situation is even worse for the toughness properties of Nitinol, where to our knowledge there exists only one paper which reports experimental measurements of its fracture toughness, K_{Ic} ; unfortunately, few details are given in this study of the material and testing procedures used [17].

Consequently, it is the primary objective of the current work to provide a comprehensive characterization of the in vitro fatigue–crack growth properties (especially at the all important near-threshold growth rates) and fracture toughness behavior in thin-walled Nitinol tubing typically used in commercial stent manufacture in simulated physiological environment, in order to realize quantifiable engineering parameters for designing against premature failure from overload and/or in vivo fatigue damage in endovascular self-expanding stents.

2. Experimental procedures

2.1. Material

Nitinol samples, with a composition of 50.8 at% Ni, were received from Nitinol Devices & Components, Inc. (Fremont, CA) in the form of compact-tension *C(T)* specimens. Nitinol tubing, similar to that used for manufacture of self-expanding stents, was cut longitudinally, and then unrolled and shape-set flat (Fig. 1). The heat treatments required to produce flattened material from the original tube configuration were similar, both in annealing time and temperature, to the commercial shape-setting procedure utilized for stent manufacture. The flattened material was laser machined into *C(T)* specimen geometries, conforming to ASTM

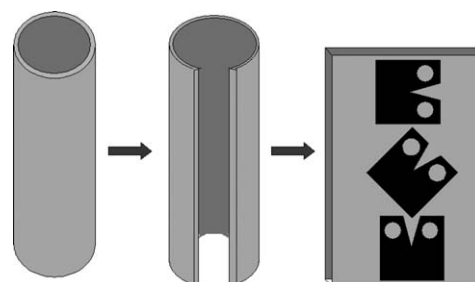


Fig. 1. Schematic illustration depicting the procedures used to produce standard compact-tension *C(T)* specimens from an originally tube-shaped geometry. The tube is first longitudinally laser cut, then unrolled through a series of shape-setting procedures, followed by laser machining of the *C(T)* specimens from the flattened configuration in a variety of angles to the drawing direction.

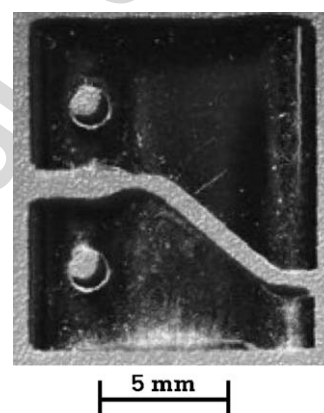


Fig. 2. A compact-tension *C(T)* specimen with pre-notch oriented in the circumferential direction and fatigue propagation path deflected $\sim 45^\circ$ to the expected mode I crack path (horizontal in this photograph).

Standard E 647 [18]; these specimens were 12 mm square with a thickness of 0.37–0.41 mm, such that all fracture mechanics testing could be performed with the same thickness configuration that is typically used for stents. Each specimen was electropolished prior to testing to minimize surface discontinuities and to produce a stent-like chemically resistant finish; the material had an austenite finish temperature of $A_f \sim 25\text{--}30^\circ\text{C}$, again consistent with commercial Nitinol stent material.

Fracture toughness tests were conducted on *C(T)* specimens that were machined with the starter notches oriented in one of three configurations: longitudinal (i.e., in the drawing direction), 45° to the drawing direction, and circumferential (Fig. 1). Conversely, the specimens used for fatigue–crack growth studies were all cut with the crack-growth direction oriented at 45° to the tube drawing direction because previous studies [19,20] on this exact material revealed that fatigue–crack extension favored this direction regardless of the initial orientation of the pre-notch (Figs. 2 and 3).

2.2. Experimental setup

All fatigue and fracture tests were conducted using an automated servo-hydraulic MTS mechanical testing system. Each sample was submerged in boiling water for 5 s immediately prior to testing to raise the sample temperature significantly above the A_f to transform any residual martensite to austenite. Samples were then allowed to equilibrate to the testing temperature, 37°C , for 10–20 min prior to starting each test. All fatigue–crack growth and fracture toughness data presented herein represent the average of at least four independent tests per condition ($n \geq 4$).

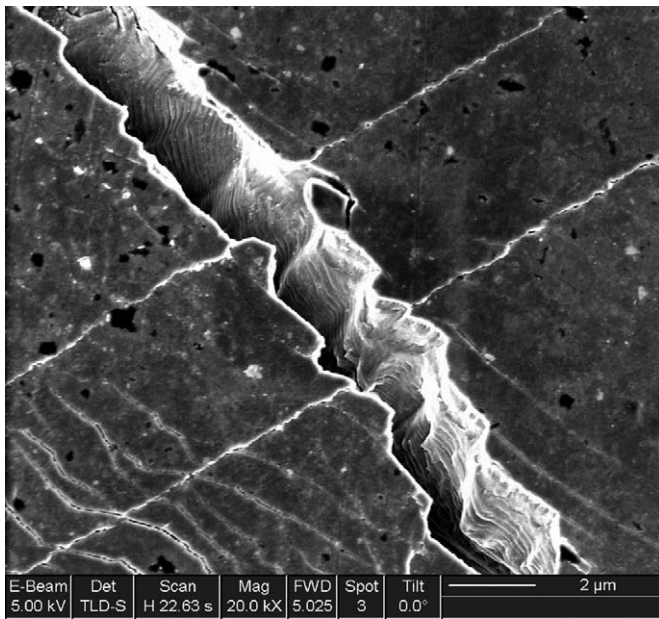


Fig. 3. Scanning electron micrograph of a kinked fatigue fracture surface showing both the primary crack and secondary microcracks angled from the energetically-favorable mode I crack path, demonstrating the influence of texture on the mechanical properties of Nitinol tube which has its lowest tensile transformational strain in the 45° plane [20] through which this sample fatigue fractured. The crack-growth direction is diagonal from top-left to bottom-right, with the applied tensile load parallel to the vertical axis ($\Delta K \sim 6 \text{ MPa}\sqrt{\text{m}}$, $da/dN \sim 10^{-7} \text{ m/cycle}$, $R = 0.1$).

In vitro fatigue-crack growth rates measurements were conducted with custom-designed grips containing a reservoir for containment of a simulated body fluid, Hanks' Balanced Saline Solution (HBSS), with laminar fluid flow controlled via a valve-regulated submerged hydraulic pump at a rate of approximately 50 ml/min across the fatigue specimens. Fluid was maintained at a temperature of 37°C and pH of 7.4 to simulate in vivo conditions. Deleterious bacterial growth was inhibited by Gentamicin at a ratio of 2 ml/l of HBSS. Testing was performed in force control at a cyclic loading frequency of 50 Hz (sine wave), except where the frequency was lowered to 1 Hz to simulate the human sinus rhythm, over a range of positive load ratios (ratio of minimum to maximum load) of $R = 0.1, 0.5$ and 0.7 ; crack lengths were continuously monitored with a capacitance-based load-line displacement gauge located on the grips. A computer-controlled feedback loop was utilized for K -control with a force-shedding rate of -0.16 mm^{-1} during the slow growth phase of the fatigue curve, i.e., near the fatigue threshold, ΔK_{th} . The value of the ΔK_{th} threshold was operationally defined, as per ASTM E647 [18], as the stress-intensity range, $\Delta K = K_{\text{max}} - K_{\text{min}}$, to give a growth rate, da/dN , of 10^{-10} m/cycle , based on linear extrapolation of data between 10^{-9} and 10^{-10} m/cycle . Stress-intensity values were computed from handbook solutions [18]. Results are characterized over a wide range of growth rates, from 10^{-10} to 10^{-6} m/cycle , and are presented either as a function of ΔK or the maximum stress intensity, K_{max} .

Fracture toughness tests were performed on nominally identical $C(T)$ specimens ($n \geq 4$) using similar crack-monitoring procedures. Specifically, samples were first fatigue pre-cracked prior to toughness testing at low R -ratio, near-threshold stress intensities ($< 5 \text{ MPa}\sqrt{\text{m}}$) to produce a nominally atomically sharp flaw, with a crack-length to sample-width ratio of $a/W \sim 0.45$. Toughness tests were then conducted in air (to allow the measurement of crack extension by telescope with a resolution of $1 \mu\text{m}$), with the temperature maintained at 37°C inside an enclosure surrounding the servo-hydraulic test system. Using a crosshead displacement rate of 400 nm/s , stable crack growth was monitored from $a/W \sim 0.45$ to 0.60 , in general accordance with ASTM E399 [21]; corresponding

measurements of the crack extension, Δa , as a function of the applied stress intensity, were then used to determine the crack-resistance or R -curves as a function of specimen orientation.

Stress intensities were again computed from handbook solutions [21]. However, as some cracks were inclined at an angle α ($\sim 25^\circ$) to the drawing direction, fracture toughness values are presented as equivalent toughness values, computed from the maximum strain-energy release rate, G , utilizing both mode I, k_{I} , and mode II, k_{II} , components, i.e.,

$$K_{\text{eq}} = [G(\alpha)E']^{1/2} = [k_{\text{I}}^2(\alpha) + k_{\text{II}}^2(\alpha)]^{1/2}, \quad (1)$$

where E' is the appropriate elastic modulus, specifically, in plane stress $E' = E$ (Young's modulus), whereas in plane strain, $E' = E/(1-\nu^2)$, where ν is Poisson's ratio. This approach compensates for the observed angled crack growth in the circumferentially oriented samples.

3. Results and discussion

3.1. In vitro fatigue-crack growth behavior

To simulate the types of fractures/failures that may result from cumulative damage events, e.g., rhythmic heartbeat, at pre-existing flaws, such as surface scratches or inclusions in the material, the in vitro fatigue-crack growth behavior of flattened Nitinol tube was measured in 37°C HBSS; results are shown for load ratios of $R = 0.1, 0.5$ and 0.7 in Figs. 4 and 5. The variation in crack-growth rates as a function of ΔK for the three load ratios at 50 Hz is shown in Fig. 4, where it can be seen that typical of most metallic and intermetallic alloys [22,23], with an increase in the (positive) load ratio, growth rates are progressively increased, particularly at near-threshold levels. This implies that growth rates depend upon K_{max} as well as ΔK , as can be seen in Fig. 5 where the growth-rate data of Fig. 4 is replotted as a function of K_{max} .

3.1.1. Fatigue thresholds

ΔK_{th} fatigue thresholds are progressively decreased at increasing load ratio, specifically by $\sim 53\%$ from $2.48 \text{ MPa}\sqrt{\text{m}}$ at $R = 0.1$ to $1.15 \text{ MPa}\sqrt{\text{m}}$ at $R = 0.7$ (Table 1). Although beyond the scope of this paper, the occurrence of such thresholds, and their decrease with increasing R , are most likely associated with the presence of crack-closure mechanisms (e.g., [22,23]) (Fig. 6). Such thresholds are of importance to stents as medical devices operating in vivo at stress intensities below ΔK_{th} will not likely experience significant subcritical cracking from surface imperfections or other pre-existing defects in the material. As for the load-ratio dependence of crack-growth rates in Nitinol, an alternative mechanistic explanation to crack closure is the occurrence of K_{max} -dominated fracture mechanisms (static modes) [24], that are typically observed in brittle materials. As instability and catastrophic fracture are approached, these mechanisms are often increasingly evident and consequently growth rates become progressively affected by the maximum stress-intensity, rather than simply the stress-intensity range. However, since in the present data, the effect of R is increasingly enhanced at lower growth rates, i.e., as K_{max} approaches the threshold

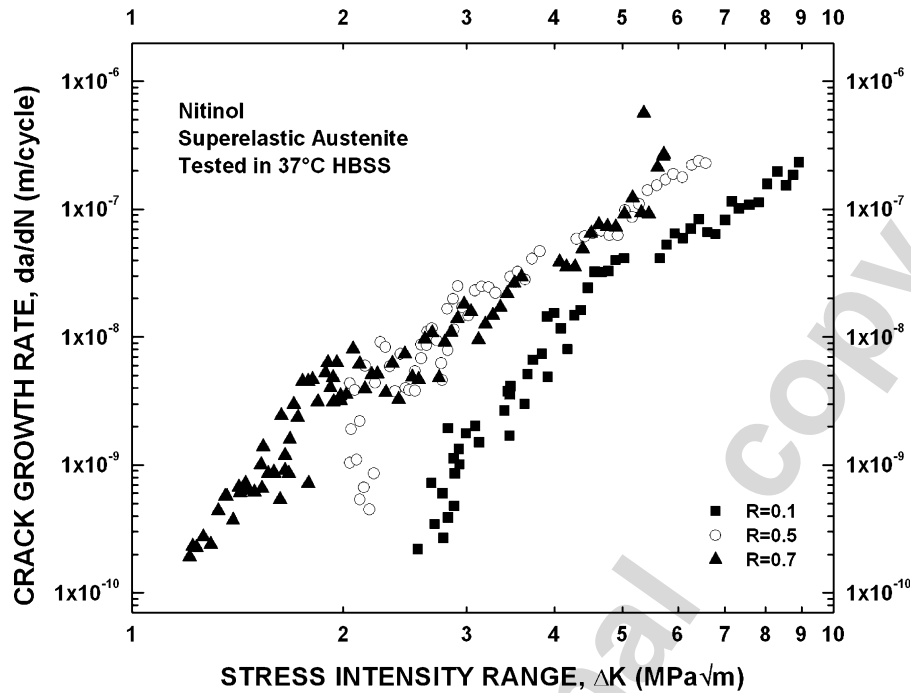


Fig. 4. Variation in in vitro fatigue–crack growth rates (da/dN) with the stress-intensity range, ΔK , in 37°C HBSS at 50 Hz test frequency for load ratios of $R = 0.1, 0.5$, and 0.7 , showing the dependencies of the fatigue threshold, ΔK_{th} , and subsequent growth rates on both ΔK and R in Nitinol tube (45° orientation). Fatigue threshold values increase from 1.15 to 2.48 $MPa\sqrt{m}$ as the R -ratio decreases from 0.7 to 0.1; $n \geq 4$.

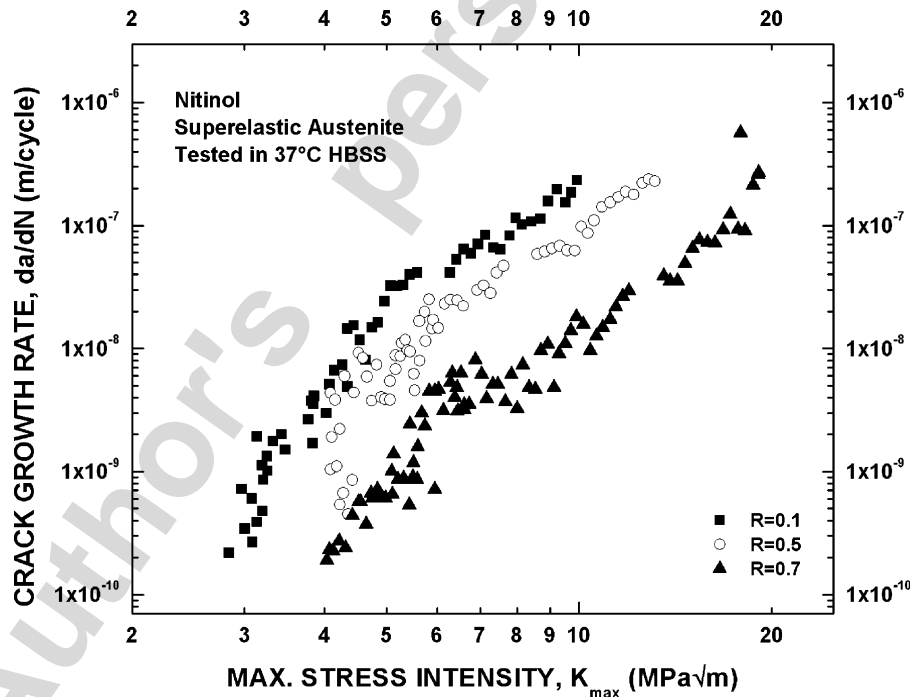


Fig. 5. In vitro fatigue–crack growth data from Fig. 2 replotted as a function of K_{max} , still demonstrates a growth-rate dependency on load ratio R , indicating that growth rates in Nitinol tube (45° orientation) have a combined dependence on both ΔK and K_{max} . This combined dependence is quantified as modified Paris-law constants that are presented in Table 1; $n \geq 4$ per condition.

rather than the fracture toughness (Fig. 4), the existence of static modes (in addition to striation growth) is unlikely to be prime explanation for load ratio effects in Nitinol. Indeed, there was little evidence of such static modes in scanning electron microscopy images of the fracture

surfaces; ductile striation growth was observed at all stress-intensity amplitudes in the higher Paris regime (Fig. 7), with the mean striation spacings corresponding well with macroscopic crack-growth rates in the scanned region.

Table 1
Paris-law fatigue-crack growth constants (defined in Eqs. (2) and (3)) and ΔK_{th} thresholds experimentally determined for flattened Nitinol tube (45° orientation) tested in Hanks' Balanced Saline Solution (HBSS) at 37 °C to simulate in vivo conditions

R-ratio	Paris constants (37 °C-HBSS/air [16])		Modified Paris constants (37 °C-HBSS/air [16])			ΔK_{th} (MPa \sqrt{m})
	<i>m</i>	<i>C</i> (m/cycle/(MPa \sqrt{m}) ^{<i>m</i>})	<i>n</i>	<i>p</i>	<i>C'</i> (m/cycle/(MPa \sqrt{m}) ^{<i>m</i>})	
0.1	4.43/4.21	$1.85 \times 10^{-11}/1.88 \times 10^{-11}$	1.87/1.53	2.56/2.68	$1.52 \times 10^{-11}/1.60 \times 10^{-11}$	2.48/2.48
0.5	3.81/3.43	$1.56 \times 10^{-10}/2.96 \times 10^{-10}$	1.25/0.75	2.56/2.68	$6.55 \times 10^{-11}/1.76 \times 10^{-10}$	2.02/1.86
0.7	3.62/3.71	$2.45 \times 10^{-10}/2.49 \times 10^{-10}$	1.06/1.03	2.56/2.68	$6.87 \times 10^{-11}/7.21 \times 10^{-11}$	1.15/1.44
0.5 (1 Hz)	3.03	2.79×10^{-10}	—	—	—	—

Results are very similar to those collected for the same material tested in air at 37 °C [16]. Experimentally determined constants are for fatigue-crack growth at 50 Hz, and show excellent correlation with crack-growth studies performed at typical in vivo frequencies (1 Hz); $n \geq 4$ for each condition, except the 1 Hz testing where $n = 1$.

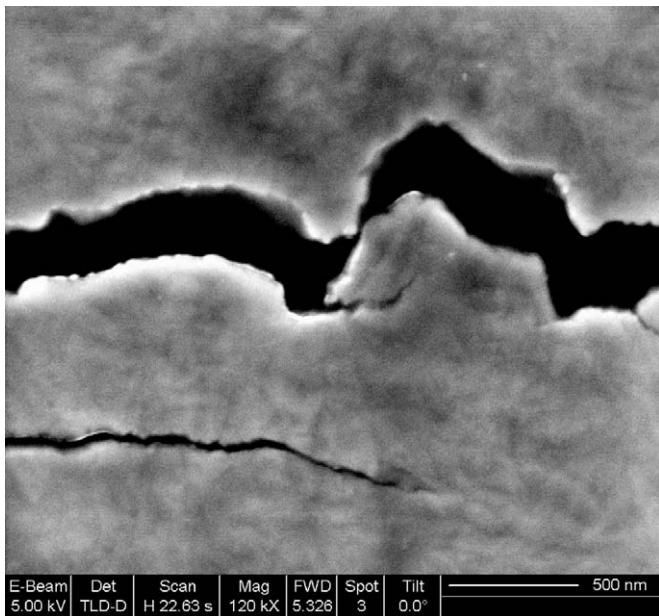


Fig. 6. Micrograph of near-threshold fatigue crack showing a tortuous crack path following the Nitinol microstructure that creates frictional interference between mating fracture surfaces; this leads to (roughness-induced) crack closure effects that ultimately can lead to arrest of the crack, e.g., at the fatigue threshold. Crack propagation is from left to right, at $\Delta K = 1.25$ MPa \sqrt{m} ($R = 0.7$).

3.1.2. Crack-growth relationships

Irrespective of the mechanism, it is important to reiterate that in vitro fatigue-crack growth rates in Nitinol are a function of both ΔK and K_{max} . This can be well described in terms of a modified Paris power-law formulation [23]. Traditionally, “mid-range” fatigue-crack growth data can be fit to Paris-law expressions, which in their simplest connotation are of the form [25]:

$$da/dN = C(\Delta K)^m, \quad (2)$$

where C and m are experimentally determined scaling constants. However, a more complete description for Nitinol can be made using a modified Paris law where growth rates are quantified in terms of both

ΔK and K_{max} [23]:

$$da/dN = C'(K_{max})^n(\Delta K)^p, \quad (3)$$

where $C' = C(1 - R)^n$ and $m = n + p$. The traditional and modified Paris-law constants (m , C , n , p , and C') for Nitinol tube are given in Table 1 and show a nominally equal dependence on both ΔK and K_{max} , although the dependence on K_{max} is higher. This trend is typical for both ductile metals and intermetallics [22,23], and it is, therefore, not surprising that Nitinol, which is an intermetallic with a B2 crystal structure in the body-temperature austenite phase, also displays roughly similar dependencies of fatigue-crack growth rates on the maximum and range of the applied stress intensities. Comparisons to crack-growth data collected for Nitinol tube samples tested in air [16] show excellent correlation with the tests conducted in a liquid environment, as indicated by the comparisons in Table 1.

3.1.3. Role of cyclic frequency

The vast majority of fatigue data on Nitinol for biomedical devices have been determined at frequencies of 30 Hz or more (e.g., [5–11,13–15]), primarily for reasons of expediency. Clearly such frequencies do not simulate physiological loading, such as human sinus rhythms, which is unfortunate since in the presence of a “corrosive” environment, fatigue-crack growth rates *per cycle* in most metallic materials are actually accelerated by lower frequencies due to an increased time period for the corrosion kinetics to be active (e.g., [26]). The implications of this are that life predictions may not be conservative when based on such higher-frequency fatigue data. Despite this, only one study [16] has addressed the influence of frequency on crack-growth behavior in Nitinol in a simulated body fluid, but crack-growth measurements were not conducted at frequencies as low as the human heartbeat (1.2 Hz).

To investigate this effect, we compare in the present work the crack-growth rate behavior in HBSS at 50 Hz (Figs. 4–5) with measurements of the corresponding growth rates at 1 Hz for specific ΔK levels. Results,

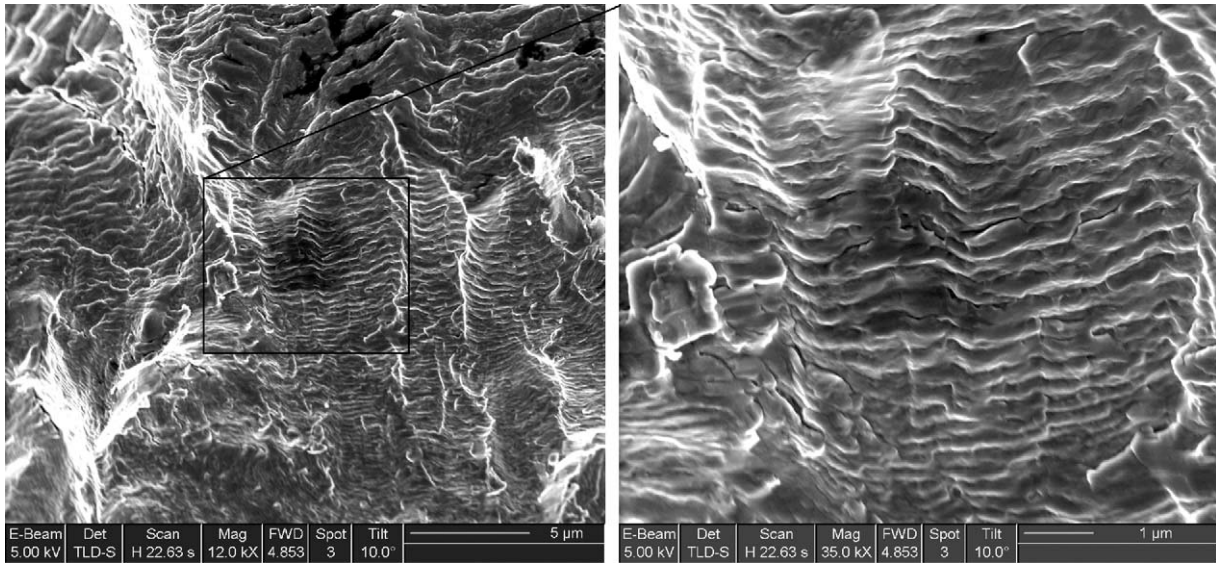


Fig. 7. Scanning electron micrographs of fatigue striations in the mid-range of growth rates (Paris) regime ($R = 0.1$, $\Delta K = 8\text{--}9 \text{ MPa}\sqrt{\text{m}}$, $da/dN = 1\text{--}2 \times 10^{-7} \text{ m/cycle}$). The fatigue striation spacing was $\sim 2\text{--}4 \times 10^{-7} \text{ m/striation}$, which corresponds well with the measured global crack-growth rates. Macroscopic fatigue crack propagation is left to right in these photo-micrographs; however, the striations in this analyzed region (near the $C(T)$ specimen surface) are oriented top to bottom due to the curvature of the crack front near the sample edges.

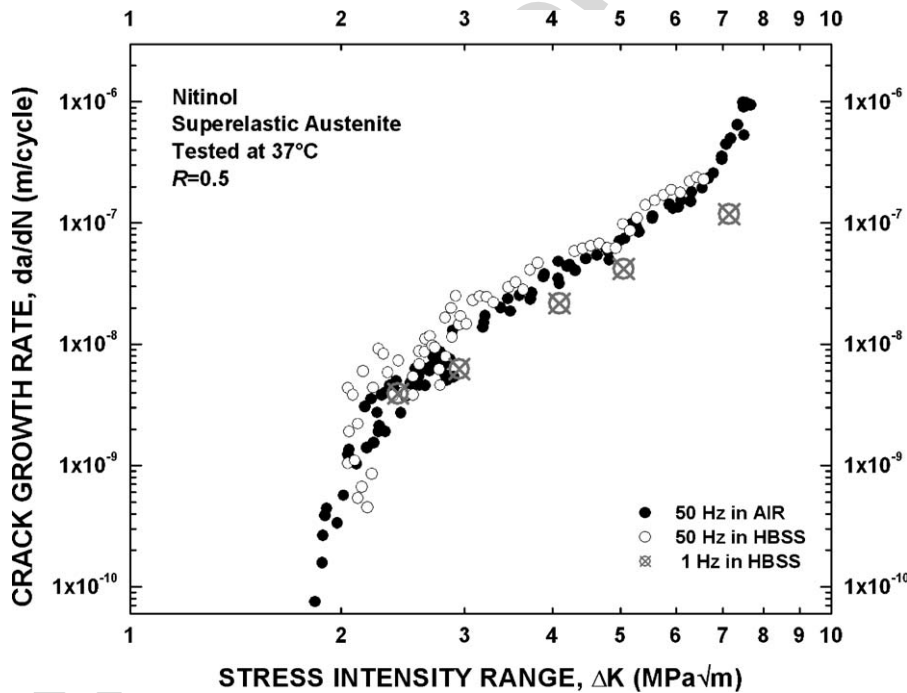


Fig. 8. Fatigue–crack growth behavior in Nitinol tube (45° orientation) at $R = 0.5$ comparing tests conducted in air at 50 Hz [16], with corresponding results in simulated body fluid (HBSS) at 50 and 1 Hz; $n \geq 4$ per condition (except at 1 Hz where $n = 1$). It is apparent that there is no significant difference in fatigue–crack growth data collected in air or in HBSS ($P = 0.53$ at 95% confidence level). Moreover, lower frequencies, which more accurately represent in vivo conditions, produce marginally slower growth rates than at higher frequencies, indicating that the higher-frequency tests that are invariably utilized may in this case provide slightly more conservative lifetime predictions for Nitinol biomedical devices.

shown in Fig. 8, indicate that at nominal ΔK levels of 2, 3, 4, 5 and $7 \text{ MPa}\sqrt{\text{m}}$, there is only a minimal difference between crack-growth rates at 1 and 50 Hz. This apparent lack of a corrosion fatigue effect in Nitinol in vitro is also evident by the fact that the Paris-law constants from the present tests at 50 Hz in HBSS are

virtually identical to those determined previously for identical tests in air [16] (Table 1). This result is consistent with the studies of Filip et al. [15] who concluded that fatigue–crack growth in thin strip Nitinol was not adversely affected by the presence of a simulated body fluid.

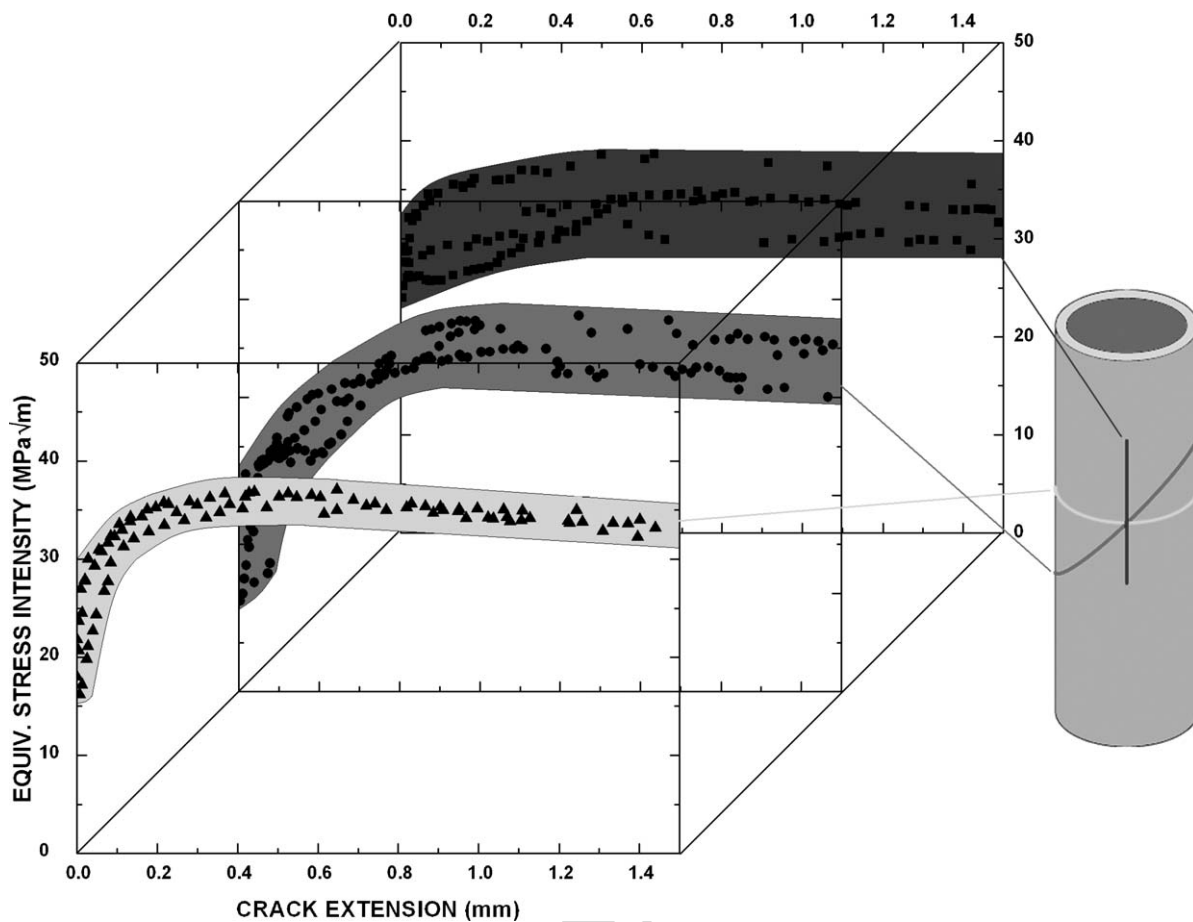


Fig. 9. Fracture toughness properties of flattened Nitinol thin-walled tubing (longitudinal, 45° and circumferential orientations) in 37 °C air, in the form of crack-resistance curves (*R*-curves), show a dependence on both crack-growth direction and the extension Δa of a non-stationary crack; $n \geq 4$ per orientation. Initial pre-notch orientations are given on the tube schematic to the right. Crack-initiation toughness values, i.e., the value of the stress intensity at $\Delta a \rightarrow 0$, range from $K_{0i} \sim 10$ to 27 MPa \sqrt{m} ; with crack advance, toughness values approach a steady-state fracture toughness of K_{ss} , ~ 34 MPa \sqrt{m} after ~ 0.4 mm crack extension.

It is interesting to note that in the present tests in addition to previously reported experiments [16], near-threshold growth rates at the lower frequency are marginally *slower* than at 50 Hz, which implies that the current policy with many stent manufacturers of using high-frequency testing may well provide a conservative basis for predicting in vivo device lifetimes. The difference in growth rates at 1 and 50 Hz is small, and could be simply associated with sample-to-sample variations; however, alternative explanations are that more crack-tip corrosion products are able to form at the lower frequency, leading to marginally enhanced (oxide-induced) crack-closure effects [27],¹ or possibly that heat, generated adiabatically due to the in situ phase transformation in Nitinol, is more effectively dissipated at the lower frequencies in the fluid environment.

¹This is actually an unlikely explanation as oxide-induced crack closure effects predominate at lower growth rates at lower ΔK levels [22], whereas the present difference in growth rates at 1 and 50 Hz is seen throughout the entire spectrum of growth rates.

Whatever the specific mechanisms, the current work (Fig. 8) clearly demonstrates for the first time that coupon or product fatigue testing at frequencies an order of magnitude higher than typical physiological (e.g., human heart beat) frequencies, does not necessarily lead to non-conservative lifetime predictions for Nitinol devices, as in vitro fatigue–crack growth rates in superelastic Nitinol tube appear to be essentially frequency-independent in simulated body fluids over the range of 1–50 Hz.

3.2. Fracture toughness behavior

To simulate the types of stent fractures and failures that may result from a single overload event, such as macroscopic bending/buckling of a superficial femoral artery stent in response to knee flexion, the fracture toughness of flattened Nitinol tube was also evaluated (Fig. 9). Toughness values were calculated in terms of an equivalent stress intensity K_{eq} , incorporating both mode I (tensile) and mode II (shear) contributions (Eq. (1)), for crack extension from a (near-threshold) fatigue-initiated pre-crack, the

latter to simulate an infinitely sharp pre-existing flaw, designed to provide the most conservative estimate of fracture toughness.

Cracks grown from pre-notches oriented in the longitudinal and 45° directions propagated by pure mode I fracture, i.e., cracks did not kink from the pre-notch orientation. However, cracks grown from pre-notches oriented in the circumferential direction kinked ~25° from the pre-notch orientation producing a mixed-mode I+II loading configuration; see Fig. 2 for an example of a 45° deflected crack. Note that in terms of a crack-driving force, the effects of these differences in crack-path orientation are accounted for in the computation of the equivalent stress intensity K_{eq} (Eq. (1)).

As toughness measurements were performed on actual stent starting material, i.e., ~400 μm thick flattened tube, deformation conditions did not constitute plane strain. Consequently, the values presented herein are not plane strain (mode I) fracture toughness K_{Ic} values. Despite this, they are accurate and entirely appropriate for the specific product form (Nitinol tube) that is used for endovascular stent manufacture. However, it should be noted here that when plane-strain conditions are not applicable, toughness values may become crack size and geometry dependent. Whereas the crack size effect is fully accounted for in the present study through the measurement of R -curves, care must be exercised in utilizing the present data for all crack configurations as the cited toughness values may be changed somewhat in different geometries [28]. However, as the present study is performed on compact-tension samples, which develop the most highly constrained (Prandtl) field at the crack tip [29], we believe that the present toughness values and R -curves can be considered as worst-case, at least for section sizes with sub-millimeter dimensions.

Results for all three sample configurations, namely circumferential, longitudinal and 45° fracture (Fig. 1) are shown in Fig. 9, and display so-called crack resistance or rising R -curve behavior, i.e., the stress intensity to initiate and sustain subcritical cracking increases with initial crack extension. The fracture toughness at the onset of crack extension, i.e., as $\Delta a \rightarrow 0$, is known as the crack-initiation toughness, K_o , and is significantly lower than the toughness required to induce significant advance of the growing crack. In the present case, the initiation toughness values for Nitinol in the circumferential, 45° and longitudinal crack-growth orientations were 16, 10 and 27 MPa√m, respectively. It is suspected that the difference in initiation toughness values as a function of crack-growth angle is due to the influence of texture in the material, as previous reports have demonstrated variable mechanical properties as a function of angle to the drawing direction in processed Nitinol tube [20] and sheet [30]. Specifically, these latter studies show that the tensile stress [30] and strain [20] required to initiate the austenite-to-martensite phase transformation are significantly lower in the 45° direction to the drawing direction, which is in good agreement

with the present results showing lowest crack-initiation toughness values in that direction. Despite significantly different crack-initiation values, all three sample configurations reach the same steady-state fracture toughness value of $K_{ss} \sim 34$ MPa√m. The presence of an R -curve in this material suggests that there are competing effects ahead of the crack tip, and in the plastic wake of the growing crack. These competing effects may be due to such factors as superelasticity, modulus mismatch between the austenite and martensite phases, and crystallographic texture.

Scanning electron microscopy of the fracture toughness specimens revealed a ductile fracture with evidence of microvoid coalescence (Fig. 10). No differences in fracture morphology were detected between the three sample configurations, or between the initiation and steady state regions.

3.3. Comparison to previous work

Previous studies of fatigue-crack growth data in superelastic austenitic bulk (9–10 mm thick) Nitinol bar reported threshold ΔK_{th} values of ~1.6 and 2 MPa√m at $R = 0.1$ [13,14], ~3 MPa√m in 200 μm thin strips at $R = 0.2$ [15], and 2.48 MPa√m in 400 μm thick flattened Nitinol tube in air at $R = 0.1$ [16]. The current test results on the 400 μm thick flattened Nitinol tube tested in HBSS at $R = 0.1$ give higher threshold values (~2.5 MPa√m) than the bulk Nitinol bar [13,14], and slightly lower values than the thin strip specimens [15]; results, however, are statistically the same as tests on similar samples tested in 37 °C air [14] ($P = 0.53$).² The traditional Paris power-law exponent, m , is slightly greater (~4) in the flattened Nitinol tube investigated in the current study (and Ref. [16]), as compared to m values of ~3 in bulk Nitinol bar [13,14] and thin strip [15]. This observation indicates that crack-growth rates (under constant cyclic loads) increase more rapidly in Nitinol tube than bar or strip, meaning that once a crack reaches steady-state growth in tube, that crack will more rapidly propagate than in other Nitinol product forms. This increased crack-growth rate is readily observed when plots of the various product forms are superimposed on each other (Fig. 11). Statistical evaluation using grouped linear regression with covariance analysis of the raw data from Ref. [14], which are visually similar to that in Ref. [15],³ was compared with the current data and showed that there is no significant correlation ($P < 0.001$ at 95% confidence level) between the crack-growth behavior of the thin-walled tube and 9–10 mm thick bar material, i.e., there is less than a 0.01% probability that the two crack-growth curves are colinear.

²Grouped linear regression with covariance analysis performed [31], indicating the probability that the two curves are statistically the same is 53% (95% confidence level).

³The raw data in Ref. [15] was not available to these authors; hence a statistical comparison could not be conducted.

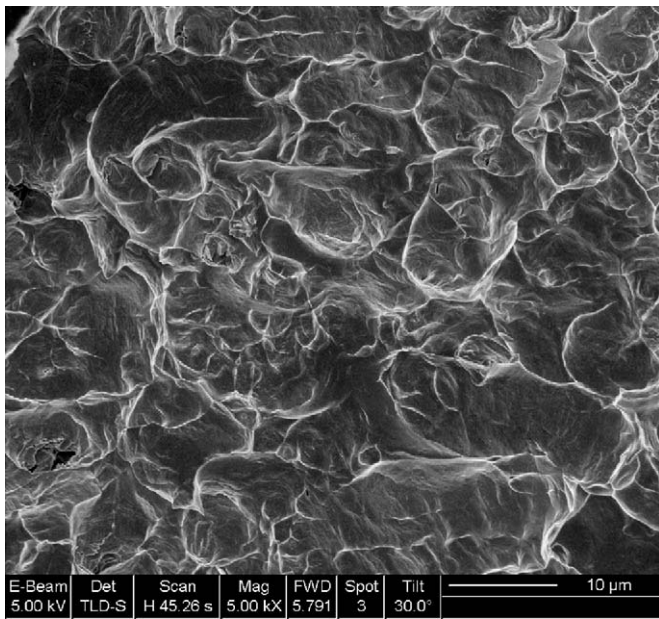


Fig. 10. Scanning electron micrograph of the overload fracture morphology, corresponding to the steady-state plateau on the R -curve ($K_{\text{c}} \sim 34 \text{ MPa}\sqrt{\text{m}}$), in a circumferentially oriented pre-notch specimen, showing ductile fracture. No difference in fractography was observed between the initiation and steady-state regions, nor between the three pre-notch orientations (longitudinal, 45° , and circumferential).

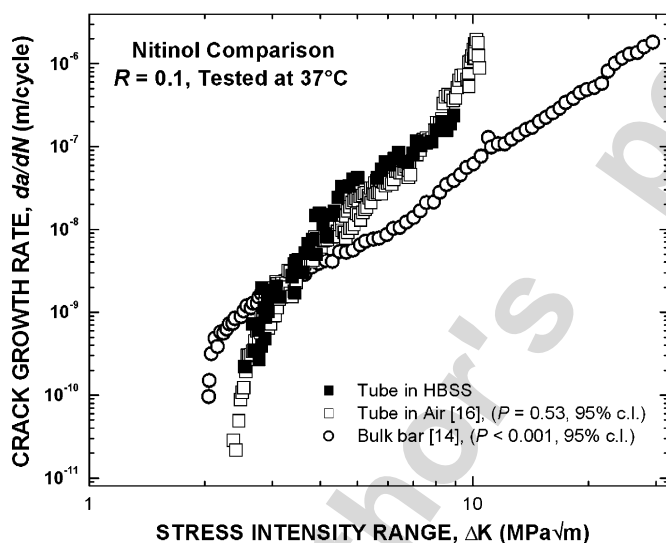


Fig. 11. Comparison of the current fatigue crack-growth behavior of Nitinol tube tested in 37°C HBSS (solid squares) at $R = 0.1$ with the same material tested in 37°C room air (hollow squares) [16], and bulk Nitinol bar (hollow circles) [14]. P -values for the hypothesis that the two curves are collinear are presented on the graph and demonstrate that the growth-rate results obtained in HBSS and air for thin-walled tube material show no significant statistical difference, whereas growth-rate results for bulk bar material vary significantly.

With respect to the toughness results, to our knowledge, there exists only one previous report of the fracture toughness of Nitinol [17], which cites a “mode I critical fracture toughness values” of $K_{\text{Ic}} = 39.2 \pm 2.8 \text{ MPa}\sqrt{\text{m}}$ for Nitinol. However, the material was of unknown original

product form and was tested with a non-standard fracture mechanics specimen geometry ($0.5 \times 3.0 \text{ mm}$ gauge cross-section with 20 mm gauge length containing a 1.6 mm deep edge notch of 0.1 mm radius). As this sample involves fracture from a blunt notch rather than an atomically sharp fatigue pre-crack, we believe that this toughness value for Nitinol is highly questionable.⁴

4. Conclusions

The damage-tolerant properties of superelastic Nitinol thin-walled tube have been investigated in simulated body fluid. Specifically, the *in vitro* fatigue-crack growth behavior, as a function of load ratio and frequency, and the fracture toughness, as a function of crack angle, have been characterized. This study represents the first report of such fracture mechanics properties relevant specifically to the Nitinol tubing used in the manufacture of many biomedical devices (e.g., stents) in a simulated body solution. Based on this study, the following specific conclusions can be drawn:

1. Fatigue-crack growth behavior in 37°C Hanks' Balanced Saline Solution (HBSS) at 50 Hz frequency was found to display a clear dependence on the load ratio, with increasing growth rates and decreasing fatigue thresholds being measured with increasing positive load ratio from 0.1 to 0.7 .
2. Fatigue-crack threshold values, ΔK_{th} , ranged from 1.15 to $2.48 \text{ MPa}\sqrt{\text{m}}$, with the lowest value being associated with a load ratio of 0.7 . Typical of intermetallic materials, crack-growth rates exhibited a similar dependency on ΔK and K_{max} .
3. Fatigue-crack growth rates at 50 Hz frequency were found to be virtually identical in 37°C air as in 37°C HBSS, indicating that at this test frequency corrosion fatigue effects in this alloy in simulated body fluids are minimal.
4. Fatigue-crack growth rates in 37°C HBSS are essentially identical at 1 and 50 Hz , indicating that the fatigue parameters quantified from 50 Hz testing represent a reasonable estimate of the crack-growth behavior at physiological loading frequencies.
5. The fracture toughness of Nitinol tube shows R -curve behavior with crack-initiation toughness significantly lower than the peak toughness value at steady state. Crack-initiation toughness values ranged from 10 to $27 \text{ MPa}\sqrt{\text{m}}$, with the lowest initiation toughness associated with fracture in the 45° -direction to the drawing axis. Steady-state fracture toughness values, conversely, were independent of orientation and were

⁴Typically, the apparent fracture toughness scales with the square root of the root radius of the stress concentrator [32]. Consequently, as shown in both metallic [32] and biological materials [33], when the fracture toughness is measured in specimens containing notches, rather than nominally atomically sharp (e.g., fatigue) pre-cracks, the resulting fracture toughness values can be highly inaccurate.

approximately constant at $\sim 34 \text{ MPa}\sqrt{\text{m}}$, which was achieved after roughly 400 μm of crack extension.

Acknowledgments

This work was supported by a gift from Nitinol Devices and Components (NDC), Inc., Fremont, California, to the University of California at Berkeley, and by the National Science Foundation under Grant no. CMS-0409294. Particular thanks are due to Drs. Tom Duerig and Alan Pelton of NDC for their financial support, supply of Nitinol samples, and for innumerable helpful discussions. The authors also acknowledge support of the National Center for Electron Microscopy, Lawrence Berkeley National Laboratory, which is supported by the U.S. Department of Energy under Contract no. DE-AC02-05CH11231.

References

- [1] Melton KN, Mercier O. Fatigue of NiTi thermoelastic martensites. *Acta Metall* 1979;27:137–44.
- [2] Harrison WJ, Lin ZC. The study of Nitinol bending fatigue. In: Proceedings of the international conference on shape memory and superelastic technologies, Pacific Grove, CA, April 2000. p. 391–396.
- [3] Tolomeo D, Davidson S, Santinoranont M. Cyclic properties of superelastic Nitinol: design implications. In: Russell SM, Pelton AR, editors. Proceedings of the international conference on shape memory and superelastic technologies. Menlo Park, CA: SMST Society, Inc.; 2000. p. 471–6.
- [4] Wurzel D, Hornbogen E. The influence of thermomechanical treatments on fatigue behavior of NiTi alloys. In: Russell SM, Pelton AR, editors. Proceedings of the international conference on shape memory and superelastic technologies. Menlo Park, CA: SMST Society, Inc.; 2000. p. 383–90.
- [5] Pelton AR, DiCello J, Miyazaki S. Optimization of processing and properties of medical-grade Nitinol wire. In: Russell SM, Pelton AR, editors. Proceedings of the international conference on shape memory and superelastic technologies. Menlo Park, CA: SMST Society, Inc.; 2000. p. 361–74.
- [6] Pelton AR, Gong XY, Duerig TW. Fatigue testing of diamond-shaped specimens. In: Duerig TW, Pelton AR, editors. Proceedings of the international conference on shape memory and superelastic technologies. Menlo Park, CA: SMST Society, Inc.; 2003. p. 293–302.
- [7] Morgan NB, Painter J, Moffat A. Mean strain effects and microstructural observations during in vitro fatigue testing of NiTi. In: Duerig TW, Pelton AR, editors. Proceedings of the international conference on shape memory and superelastic technologies. Menlo Park, CA: SMST Society, Inc.; 2003. p. 303–10.
- [8] Eggeler G, Hornbogen E, Yawny A, Heckmann A, Wagner M. Structural and functional fatigue of NiTi shape memory alloys. *Mater Sci Eng A* 2004;378:24–33.
- [9] Wagner M, Sawaguchi T, Kausträter G, Höffken D, Eggeler G. Structural fatigue of pseudoelastic NiTi shape memory wires. *Mater Sci Eng A* 2004;378:105–9.
- [10] Prymak O, Klocke A, Kahl-Nieke B, Epple M. Fatigue of orthodontic nickel–titanium (NiTi) wires in different fluids under constant mechanical stress. *Mater Sci Eng A* 2004;A378:110–4.
- [11] Fife D, Gambarini G, Britto LR. Cyclic fatigue testing of ProTaper NiTi rotary instruments after clinical use. *Oral Surg, Oral Med, Oral Pathol, Oral Radiol Endodont* 2004;97:251–6.
- [12] Marrey RV, Burgermeister R, Grishaber RB, Ritchie RO. Fatigue and life prediction for cobalt–chromium stents: a fracture mechanics analysis. *Biomaterials* 2006;27:1988–2000.
- [13] Dauskardt RH, Duerig TW, Ritchie RO. Effects of in situ phase transformation on fatigue–crack propagation in titanium–nickel shape-memory alloys. In: Otsuka K, Shimizu K, editors. Shape Memory Materials, Proceedings of the MRS International Meeting on Advanced Materials, vol. 9. Pittsburgh, PA: Materials Research Society; 1989. p. 243–9.
- [14] McKelvey AL, Ritchie RO. Fatigue–crack growth behavior in the superelastic and shape-memory alloy Nitinol. *Metall Mater Trans A* 2001;32A:731–43.
- [15] Filip P, Paliwal M, Mazanec K. Fatigue behavior of pseudoelastic TiNi thin strips in air and body fluid simulated environments. *Z Metall* 2004;95:356–61.
- [16] Stankiewicz JM, Robertson SW, Ritchie RO. On the fatigue–crack growth properties of thin-walled superelastic austenitic Nitinol tube for endovascular stents. *J Biomed Mater Res A*. 2006, accepted for publication.
- [17] He JY, Gao KW, Su YJ, Qiao LJ, Chu WY. The role of hydride, martensite and atomic hydrogen in hydrogen-induced delayed fracture of TiNi alloy. *Mater Sci Eng* 2004;A364:333–8.
- [18] American Society of Testing Materials. International, Subcommittee E08.06, “standard test method for measurement of fatigue crack growth rates”. ASTM Book of Standards, v.3.01, Standard E 647, 2005.
- [19] Robertson SW, Stankiewicz J, Gong XY, Ritchie RO. Cyclic fatigue of Nitinol. In: Mertmann M, editor. Proceedings of the international conference on shape memory and superelastic technologies. Materials Park, OH: ASM Intl; 2004. p. 79–88.
- [20] Robertson SW, Gong XY, Ritchie RO. Effect of product form and heat treatment on the crystallographic texture of austenitic Nitinol. *J Mater Sci* 2006;41:621–30.
- [21] American Society of Testing Materials. International, Subcommittee E08.06, “standard test method for measurement of the plane strain fracture toughness in metallic materials”. ASTM Book of Standards, v.3.01, Standard E 399, 2005.
- [22] Ritchie RO. Mechanisms of fatigue crack propagation in metals, ceramics and composites: role of crack-tip shielding. *Mater Sci Eng A* 1988;103:15–28.
- [23] Ritchie RO. Mechanisms of fatigue–crack propagation in ductile and brittle solids. *Int J Fract* 1999;100:55–83.
- [24] Ritchie RO, Knott JF. Mechanisms of fatigue crack growth in low alloy steel. *Acta Metall* 1973;21:639–48.
- [25] Paris PC, Erdogan F. A critical analysis of crack propagation laws. *J Basic Eng, Trans ASME, D* 1963;85:528–34.
- [26] Bartlett ML, Hudak Jr SJ. The influence of frequency-dependent crack closure on corrosion fatigue–crack growth. In: Kitagawa H, Tanaka T, editors. Fatigue 90, vol. 3. Birmingham, UK: Materials & Components Engineering Publications; 1990. p. 1783–8.
- [27] Suresh S, Zamiski GF, Ritchie RO. Oxide-induced crack closure: an explanation for near-threshold corrosion fatigue crack growth behavior. *Metall Trans A* 1981;12A:1435–43.
- [28] Anderson TL. Fracture mechanics: fundamentals and applications, third ed. Boca Raton, FL: CRC Press; 2004.
- [29] Knott JF. Fundamentals of fracture mechanics. UK: Butterworths; 1973.
- [30] Gao S, Yi S. Experimental study on the anisotropic behavior of textured NiTi pseudoelastic shape memory alloys. *Mater Sci Eng A* 2003;362:107–11.
- [31] Armitage P, Berry G. Statistical methods in medical research, third ed. Oxford: Blackwell Publishing; 1994.
- [32] Ritchie RO, Horn RN. Further considerations on the inconsistency of toughness evaluation of AISI 4340 steel austenitized at increasing temperatures. *Metall Trans A* 1978;9A:331–41.
- [33] Imbeni V, Nalla RK, Bosi C, Kinney JH, Ritchie RO. In vitro fracture toughness of human dentin. *J. Biomed Mater Res A* 2003; 66A:1–9.